Arginine 49 Is a Bifunctional Residue Important in Catalysis and Biosynthesis of Monomeric Sarcosine Oxidase: A Context-Sensitive Model for the Electrostatic Impact of Arginine to Lysine Mutations[†,‡]

Alshaimaa Hassan-Abdallah,[§] Guohua Zhao,[§] Zhi-wei Chen,[||] F. Scott Mathews,[||] and Marilyn Schuman Jorns*[,§]

Department of Biochemistry and Molecular Biology, Drexel University College of Medicine, Philadelphia, Pennsylvania 19102, and Department of Biochemistry and Molecular Biophysics, Washington University School of Medicine, St. Louis, Missouri 63110

Received November 28, 2007; Revised Manuscript Received December 20, 2007

ABSTRACT: Monomeric sarcosine oxidase (MSOX) contains covalently bound FAD and catalyzes the oxidative demethylation of sarcosine (*N*-methylglycine). The side chain of Arg49 is in van der Waals contact with the *si* face of the flavin ring; sarcosine binds just above the *re* face. Covalent flavin attachment requires a basic residue (Arg or Lys) at position 49. Although flavinylation is scarcely affected, mutation of Arg49 to Lys causes a 40-fold decrease in k_{cat} and a 150-fold decrease in $k_{cat}/K_{m\ sarcosine}$. The overall structure of the Arg49Lys mutant is very similar to wild-type MSOX; the side chain of Lys49 in the mutant is nearly congruent to that of Arg49 in the wild-type enzyme. The Arg49Lys mutant exhibits several features consistent with a less electropositive active site: (1) Charge transfer bands observed for mutant enzyme complexes with competitive inhibitors absorb at higher energy than the corresponding wild-type complexes. (2) The pK_a for ionization at N(3)H of FAD is more than two pH units higher in the mutant than in wild-type MSOX. (3) The reduction potential of the oxidized/radical couple in the mutant is 100 mV lower than in the wild-type enzyme. The lower reduction potential is likely to be a major cause of the reduced catalytic activity of the mutant. Electrostatic interactions with Arg49 play an important role in catalysis and covalent flavinylation. A context-sensitive model for the electrostatic impact of an arginine to lysine mutation can account for the dramatically different consequences of the Arg49Lys mutation on MSOX catalysis and holoenzyme biosysnthesis.

Monomeric sarcosine oxidase (MSOX)[1] catalyzes the oxygen-dependent demethylation of sarcosine (*N*-methylglycine), producing formaldehyde, glycine, and hydrogen peroxide as reaction products. The enzyme will also oxidize other amino acids containing a secondary amino group (e.g., L-proline, *N*-methyl-L-alanine) (*1, 2*). MSOX contains covalently bound flavin (8α-*S*-cysteinyl-FAD) (*3*) and is a prototypical member of a family of amine-oxidizing enzymes that contain covalently bound FAD as the only prosthetic group. Other family members include *N*-methyltryptophan oxidase, nikD, pipecolate oxidase, and fructosyl amino acid oxidase (*4–7*). Studies with the apoenzyme of wild-type MSOX show that covalent flavin attachment occurs in an autocatalytic reaction that requires only FAD (*8*).

MSOX binds the unreactive zwitterionic form of its amino acid substrates. Substrate activation is achieved by inducing a large decrease in the pK_a of the bound zwitterion, accompanied by the formation of a charge transfer complex between the electron-rich amino acid anion and oxidized FAD. Conversion of the charge transfer complex to reduced enzyme occurs in a spectroscopically isosbestic reaction that provides no evidence for the formation of a redox intermediate (*9–11*), a finding consistent with a hydride transfer mechanism. *N*-(Cyclopropyl)glycine acts as a suicide substrate that inactivates MSOX in a mechanism that involves single electron transfer (*12, 13*). However, the inactivation rate is $\sim 10^5$-fold slower than sarcosine oxidation, indicating that substrate oxidation is unlikely to involve the formation of flavin or substrate radicals as intermediates.

High-resolution crystal structures have been determined for free MSOX and complexes with competitive inhibitors including pyrrole-2-carboxylate (PCA), an aromatic analogue of the amino acid substrate L-proline (*1, 14*). PCA and other inhibitors are bound in an active site cavity located just above the *re* face of the flavin ring. The carboxylate of PCA forms hydrogen bonds to the side chains of Lys348 and Arg52, and its pyrrole nitrogen is hydrogen bonded to the carbonyl oxygen of Gly344. The flavin ring separates the active site

[†] This work was supported in part by Grant GM 31704 (to M.S.J.) from the National Institutes of Health.

[‡] Crystallographic coordinates have been deposited in the Protein Data Bank under the file names 3BHF for the PEG-crystallized and 3BHK for the phosphate-crystallized Arg49Lys mutants of MSOX.

* To whom correspondence and requests for reprints should be addressed. Phone: (215) 762-7495. Fax: (215) 762-4452. E-mail: marilyn.jorns@drexelmed.edu.

[§] Drexel University College of Medicine.

[||] Washington University School of Medicine.

[1] Abbreviations: MSOX, monomeric sarcosine oxidase; FAD, flavin adenine dinucleotide; PCA, pyrrole-2-carboxylate; MTA, methylthioacetate.

10.1021/bi702351v CCC: $40.75
Published on Web 02/06/2008

cavity from Arg49, a residue whose side chain is in van der Waals contact with the *si* face of the flavin ring.

Our recent studies show that Arg49 is essential for covalent flavin attachment (*15*). Substitution of Arg49 with a neutral residue blocks covalent flavinylation; the mutant apoproteins retain the ability to bind flavin noncovalently. Replacement of Arg49 with Lys yields a preparation that contains both holoenzyme (with covalently bound FAD) and apoprotein. *In vitro* reconstitution of apoArg49Lys is readily achieved in a reaction that exhibits kinetic parameters similar to those observed for flavinylation of wild-type apoMSOX. Surprisingly, although covalent flavin attachment is scarcely affected, mutation of Arg49 to Lys results in a substantial decrease in catalytic activity. The specific activity of the Arg49Lys holoenzyme is only 4% of that observed with wild-type MSOX, suggesting that Arg49 may also play an important role in sarcosine oxidation.

In this paper we investigate the biochemical and structural properties of the Arg49Lys MSOX mutant. The studies provide insight regarding the potential electrostatic impact of changing arginine to lysine, a substitution generally regarded as conservative.

EXPERIMENTAL PROCEDURES

Materials. Amplex Red was obtained from Molecular Probes. Horseradish peroxidase and *o*-dianisidine were purchased from Sigma. Methylthioacetate, pyrrole-2-carboxylate, and methyl viologen were obtained from Aldrich. Methylene blue and phenazine methosulfate were from Fluka. 5-Deazariboflavin was previously synthesized in this laboratory, according to the method of O'Brien et al. (*16*). Pyocyanine was prepared by photochemical oxidation of phenazine methosulfate (0.75 mM in water) according to previously described procedures (*17, 18*) and used without further purification. Purified xanthine oxidase was a generous gift from Dr. Russ Hille.

Enzyme Expression and Purification. Wild-type MSOX and the Arg49Lys mutant were expressed and purified as previously described (*3, 8, 15*). Catalytic activity was monitored by using a horseradish peroxidase-coupled assay with Amplex Red (*19*) or *o*-dianisidine (*2*) as the chromogenic substrate. The concentration of the wild-type or Arg49Lys mutant holoenzyme was estimated on the basis of flavin absorbance [ϵ_{454} = 12200 M^{-1} cm^{-1} (wild type); ϵ_{450} = 13700 (Arg49Lys)] (*3, 15*).

Steady-State Kinetic Studies. Steady-state kinetic studies with Arg49Lys or wild-type MSOX at various concentrations of sarcosine and oxygen were conducted in 100 mM potassium phosphate buffer, pH 8.0, at 25 °C using a horseradish peroxidase coupled-assay with *o*-dianisidine as the chromogenic substrate and screw-cap cuvettes (Spectrocell) equipped with a Teflon−silicon membrane. The sealed cuvettes were equilibrated at 25 °C with water-saturated gas mixtures containing 5%, 10%, 21%, 44%, or 100% oxygen (balance nitrogen), as previously described (*2*). Steady-state kinetic parameters were estimated by fitting an equation for a sequential mechanism (eq 1, A = sarcosine, B = oxygen) to the data.

$$v = \frac{V_{max}[A][B]}{K_{ia}K_b + K_a[B] + K_b[A] + [A][B]} \quad (1)$$

Spectroscopy. Absorption spectra were recorded using an Agilent Technologies 8453 diode array or a Perkin-Elmer Lambda 25 spectrophotometer. Dissociation constants for spectrally detectable complexes formed with Arg49Lys and methylthioacetate or pyrrole-2-carboxylate were determined by fitting a theoretical binding curve to absorbance changes observed at 515 or 568 nm, respectively. Spectra corresponding to 100% complex formation were calculated as previously described (*11*). Special cuvettes with two side arms were used for anaerobic experiments. The cuvettes were made anaerobic by bubbling argon through protein-free solutions in the main compartment or over the surface of small aliquots of enzymes in the side arms. Photoreduction of Arg49Lys was conducted by irradiating an anaerobic sample of the mutant enzyme with two 15 W blue-black fluorescent tubes.

Determination of Reduction Potentials. The redox potentials of the Arg49Lys mutant were determined using the xanthine/xanthine oxidase method described by Massey (*20*). Reactions were conducted at 25 °C in 50 mM potassium phosphate buffer, pH 8.0, containing 20 μM methyl viologen (mediator dye), 1 μM riboflavin, 60 μM EDTA, 300 μM xanthine, 20 μM methylene blue or 60 μM pyocyanine (indicator dye), and a catalytic amount of xanthine oxidase. The main compartment of the anaerobic cuvette contained all nonprotein components; xanthine oxidase and the Arg49Lys MSOX mutant were placed in separate side arms. After degassing, spectra were recorded before and after tipping the MSOX mutant into the main compartment. The reaction was then started by adding xanthine oxidase, and spectra were recorded over a period of at least 230 min. The extent of reduction of methylene blue or pyocyanine was determined on the basis of the decrease in absorption due to the oxidized dye at 665 or 688 nm, respectively. The oxidized and radical forms of Arg49Lys exhibit maxima at 450 and 387 nm, respectively, and an isosbestic point at 406 nm. The concentrations of the oxidized (OX), radical (RAD), and fully reduced (RED) forms of the Arg49Lys mutant were determined on the basis of the absorbance of the reaction mixture at 450, 387, and 406 nm (corrected for the contribution from the oxidized and reduced indicator dye) by using extinction coefficients determined for each enzyme redox species at the indicated wavelengths. Extinction coefficients for the three redox forms of the Arg49Lys mutant were calculated using a value previously determined for the oxidized form at 450 nm (*15*) and data obtained in this study for the photoreduction of the mutant, a reaction that proceeds with quantitative formation of a radical intermediate. The Nernst equation was then used to calculate reduction potentials by plotting log([OX]/[RAD]) or log([RAD]/[RED]) of the mutant unknown versus log[dye_{ox}]/[dye_{red}] of the indicator dye, using −20.0 and −87.6 mV as the known midpoint potentials of methylene blue and pyocyanine, respectively, at pH 8.0 (*21, 22*).

The same procedure was used to determine the reduction potential for the OX/RAD couple (E_1) with wild-type MSOX except that 20 μM toluylene blue was used as the indicator dye (E_m = 81.3 mV, pH 8.0) (*21*).

Crystallization and Data Collection. The isolated Arg49Lys mutant was reconstituted with excess FAD to increase the holoenzyme content of the preparation, as described by Hassan-Abdallah et al. (*15*). Crystals of the reconstituted

Table 1: Data Collection and Structure Determination of the Arg49Lys MSOX Mutant Crystals

crystal	phosphate grown	PEG grown
Data Collection		
resolution (Å)	30–1.70	30–2.10
no. of reflections	74292	43803
completeness (all/outer 0.05 Å shell, %)	94.1/82.2	93.2/74.0
R_{merge}[a] (all/outer)	0.063/0.264	0.086/0.348
$\langle I\rangle/\sigma$[b] (all/outer)	14.9/2.3	12.0/2.0
redundancy (all/outer shell)	3.3/2.1	3.5/2.4
Refinement		
no. of reflections used	73282	42142
no. of reflections, working set	69539	40033
no. of reflections, test set	3743	2109
R[c]	0.172	0.202
R_{free}[d] (all/outer 0.05 Å shell)	0.208	0.251
no. of protein atoms (non-H)[e]	6014	5950
⟨B⟩ (Å^2)	21.3	37.6
no. of alternate conformers	0	3
no. of FAD atoms (non-H)[e]	106	106
⟨B⟩ (Å^2)	14.7	B
no. of chloride ions[e]	2	2
⟨B⟩ (Å^2)	16.0	44.1
no. of glycerol molecules	2	0
⟨B⟩ (Å^2)	33.8	
no. of solvent molecules[e]	658	350
⟨B⟩ (Å^2)	34.5	38.6
RMSD		
bonds (Å)	0.011	0.010
angles (deg)	1.67	1.60
ΔB (main−main, Å^2)	1.35	2.51
ΔB (main−side, Å^2)	2.80	1.78
ΔB (side−side, Å^2)	2.50	2.51

[a] $R_{merge} = \sum_h\sum_i I(h) - I_i(h)/\sum_h\sum_i I_i(h)$, where $I_i(h)$ and $I(h)$ are the ith and mean measurements of reflection h. [b] $\langle I\rangle/\sigma$ is the average signal to noise ratio for merged reflection intensities. [c] $R = \sum_h(F_o - F_c)/\sum_h F_o$, where F_o and F_c are the observed and calculated structure factor amplitudes of reflection h. [d] R_{free} is the test reflection data set, about 10% selected randomly for cross-validation during crystallographic refinement (*26*). [e] Per asymmetric unit which contains two molecules of MSOX.

enzyme were grown under two conditions (phosphate and PEG) by the sitting drop method as described previously (*14*). Equal volumes of 5 μL each of protein solution (10 mg/mL in 20 mM Tris-HCl, pH 8.0) and reservoir solution (1.8 M sodium/potassium phosphate buffer, pH 7.0, for "phosphate" and ~20% PEG3350 and 200 mM $NaNO_3$, pH 6.8, for "PEG") were mixed and allowed to equilibrate. X-ray data were recorded from a single crystal from each condition at 100 K using glycerol as a cryoprotectant on an ADSC Quantum-315 CCD detector at Biocars Beamline 14-BM-C at the Advanced Photon Source, Argonne, IL. The crystals were monoclinic, space group $P2_1$, with unit cell parameters $a = 72.65$ Å, $b = 69.65$ Å, $c = 73.36$ Å, and $\beta = 93.74°$ for "phosphate" and $a = 72.35$ Å, $b = 70.46$ Å, $c = 79.59$ Å, and $\beta = 96.77°$ for "PEG". Both crystals contained two protein molecules per asymmetric unit. Spot integration and data scaling were carried out using HKL 2000 (*23*). The data collection statistics are summarized in Table 1.

Structure Determination and Refinement. The initial coordinates of the "phosphate" crystal were obtained by direct refinement of the wild-type MSOX structure (PDB code 2GB0) while those for the "PEG" crystal were obtained by molecular replacement using MOLREP (*24*) since the unit cell parameters were significantly different from those of the native structure.

The refinement and electron density map calculations were carried out using CNS (*25*), and 5% of the reflections were selected randomly and set aside as a test set for cross-validation (*26*). Reflections from 40 Å to the diffraction limit recorded for each data set (1.70 and 2.10 Å resolution, respectively; see Table 1) were included in the refinements, and a bulk solvent correction was applied (*27*). Noncrystallographic symmetry (NCS) restraints were applied to the two protein molecules in each asymmetric unit during refinement (with NCS weights set to 300 for both main and side chain atoms) except for two short polypeptide segments plus four side chains, all near the protein surface and which consistently differed from each other in the two subunits. The differences between *B*-factors for bonded atoms were restrained using target standard deviations of 1.5 Å^2 for main chain and 2.0 Å^2 for side chain atoms, and reflections with $\sigma(I) < 0.0$ were omitted. Model building and analysis of the structures were carried out on a Silicon Graphics workstation using Turbo-Frodo (*28*). Rigid body refinement followed by several cycles of positional, temperature factor and simulated annealing refinement and then interactive model building and automatic solvent placement with manual examination were carried out. This procedure utilized electron density difference maps calculated with Fourier coefficients ($2F_o - F_c$) and ($F_o - F_c$), where F_o and F_c are the observed and calculated structure factors, respectively. The final refinement statistics are shown in Table 1.

Structural Calculations and Drawings. Structural diagrams were rendered using PYMOL (http://www.pymol.org).

RESULTS

Catalytic Properties of Arg49Lys. The steady-state kinetic properties of the mutant were investigated by measuring apparent turnover rates at various concentrations of sarcosine and oxygen. Double reciprocal plots of reaction rate versus sarcosine at different oxygen concentrations or versus oxygen at different sarcosine concentrations are linear and intersect to the left of the *Y*-axis and below the *X*-axis (Figure 1). These features are consistent with a mechanism where oxygen reacts with the reduced enzyme before the imine product is released (Scheme 1), as observed with wild-type MSOX (*2*). The steady-state kinetic parameters listed in Table 2 were obtained by fitting an equation for a sequential mechanism to the data. The apparent second-order rate constant for the reaction of oxidized mutant enzyme with sarcosine ($k_{cat}/K_{m\ sarcosine}$) is about 150-fold slower than observed with the wild-type enzyme. The turnover rate of the mutant at saturating oxygen and sarcosine concentrations (k_{cat}) is about 40-fold slower than that of the wild-type enzyme. The mutation appears to have a smaller effect on the reaction of the reduced enzyme·imine complex with oxygen, as judged by the 12-fold lower value obtained for $k_{cat}/K_{m\ oxygen}$ as compared with wild-type MSOX.

Inhibitor Binding to the Arg49Lys Mutant. Studies were conducted with substrate analogues that are known to perturb the visible absorption spectrum of wild-type MSOX. Methylthioacetate (MTA, $CH_3SCH_2CO_2^-$) is a sarcosine analogue in which the substrate nitrogen is replaced by sulfur. The Arg49Lys mutant forms a complex with MTA that exhibits a new absorption band in the long-wavelength region (Figure 2A), a feature diagnostic of charge transfer interaction. Wild-

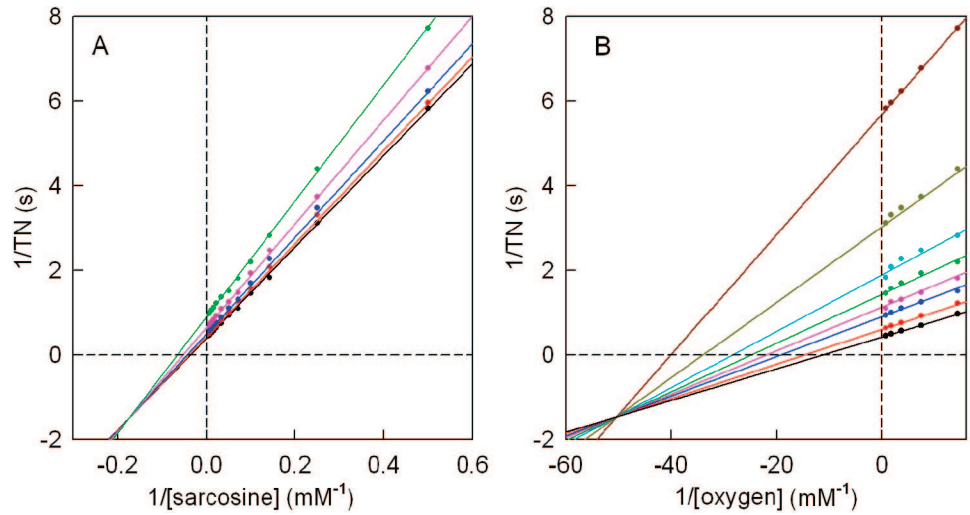

FIGURE 1: Steady-state kinetic analysis of sarcosine oxidation by the Arg49Lys mutant. Reactions were conducted in 100 mM potassium phosphate buffer, pH 8.0, at 25 °C. Panel A: Data obtained at 0.069, 0.13, 0.27, 0.57, and 1.28 mM oxygen are shown by the green, magenta, blue, red, and black circles, respectively. Panel B: Data obtained at 2, 4, 7, 10, 14, 20, 45, and 204 mM sarcosine are shown by dark red, dark yellow, cyan, green, magenta, blue, red, and black circles, respectively. For clarity, the figure does not include data at five sarcosine concentrations (60, 78, 99, 130, and 166 mM) that lie in between the two highest concentrations shown in the figure. The solid lines in panels A and B were obtained by fitting eq 1 to the data.

Scheme 1: Proposed Steady-State Kinetic Mechanism for Sarcosine Oxidation by MSOX

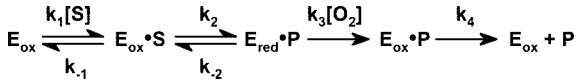

Table 2: Steady-State Kinetic Parameters[a]

	Arg49Lys	wild-type MSOX
k_{cat} (s^{-1})	2.70 ± 0.02	101 ± 2 (117 ± 3)
$K_{m\ sarcosine}$ (mM)	28.8 ± 0.07	7.6 ± 0.4 (9.4 ± 0.4)
$K_{m\ oxygen}$ (mM)	0.098 ± 0.002	0.29 ± 0.01 (0.35 ± 0.02)
$K_{i\ sarcosine}$ (mM)	6 ± 1	0.4 ± 0.2 (0.6 ± 0.3)
$k_{cat}/K_{m\ sarcosine}$ ($mM^{-1}\ s^{-1}$)	0.094 ± 0.007	13.3 ± 0.7
$k_{cat}/K_{m\ oxygen}$ ($mM^{-1}\ s^{-1}$)	28 ± 2	350 ± 10

[a] Steady-state kinetic parameters were determined in 100 mM potassium phosphate buffer, pH 8.0, at 25 °C, as described in Experimental Procedures and the caption to Figure 1. Values in parentheses were previously obtained by Wagner and Jorns under the same conditions (*2*).

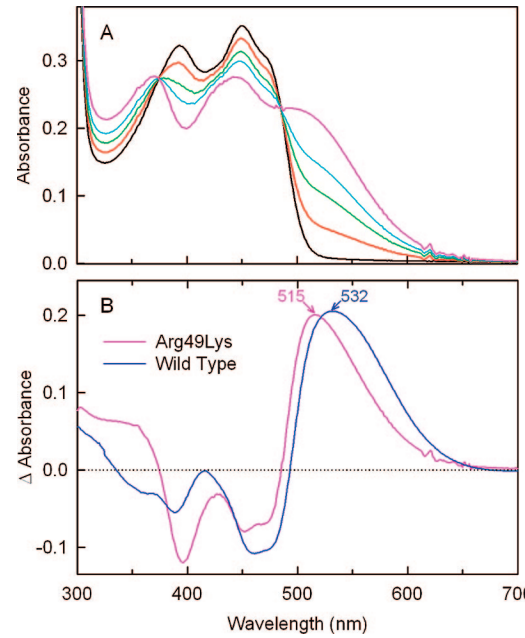

FIGURE 2: Spectral titration of the Arg49Lys mutant with methylthioacetate (MTA). Panel A shows absolute absorption spectra. The black curve is the free Arg49Lys mutant (25.7 μM) in 100 mM potassium phosphate buffer, pH 8.0, at 25 °C. The red, green, and cyan curves were recorded after addition of 16.0, 49.5, and 112 mM MTA, respectively. The magenta curve is the spectrum calculated for 100% complex formation, as described in Experimental Procedures. Panel B compares difference spectra calculated for 100% complex formation with Arg49Lys (magenta curve) and the wild-type enzyme (blue curve). The data for the wild-type enzyme were taken from Wagner et al. (*1*) and are normalized to the same concentration as the mutant.

type MSOX also forms a charge transfer complex with MTA (*1*). However, the charge transfer band with the mutant enzyme is shifted to shorter wavelengths (higher energy) than with wild-type MSOX, as judged by the position of the long-wavelength bands in the corresponding difference spectra (λ_{max} = 515 and 532 nm, respectively) (Figure 2B). The Arg49Lys mutation also caused a 20-fold decrease in the stability of the MTA complex, as estimated by comparison of its dissociation constant with that reported for wild-type MSOX (Table 3).

Pyrrole-2-carboxylate (PCA) is an aromatic analogue of L-proline (an alternate substrate for MSOX) and forms a charge transfer complex with wild-type MSOX (*1*). A charge transfer complex is also observed with the Arg49Lys mutant, but the charge transfer band is again shifted to shorter wavelengths as compared with wild-type MSOX (λ_{max} = 558 and 608 nm, respectively) (Figure 3). The dissociation constant for the PCA complex with the mutant enzyme is 40-fold larger than observed with the wild-type enzyme (Table 3).

Effect of the Arg49Lys Mutation on the pK_a for Flavin Ionization. Ionization at the N(3)H position in the flavin ring is readily detected by spectrophotometric titration because it results in a diagnostic hypsochromic shift of the higher energy

Table 3: Comparison of Biophysical Properties of the Active Site in the Arg49Lys Mutant with Wild-Type MSOX

	Arg49Lys	wild type
enzyme·MTA complex		
K_d (mM)	54 ± 1	2.6[a]
$\lambda_{max\ (CT\ band)}$ (nm)	515	532[a]
enzyme·PCA complex		
K_d (mM)	58 ± 5	1.37[a]
$\lambda_{max\ (CT\ band)}$ (nm)	558	608[a]
pK_a [FAD N(3)H]	10.4 ± 0.1	8.3[a]
reduction potential (mV)		
E_1 (OX/RAD)	−21.0 ± 0.1	+82.2 ± 0.3 (+79.5 ± 0.2)[b]
E_2 (RAD/RED)	−47.4 ± 0.2	

[a] Data with wild-type MSOX were reported by Wagner et al. (*1*). [b] Value reported by Zhao et al. (*31*).

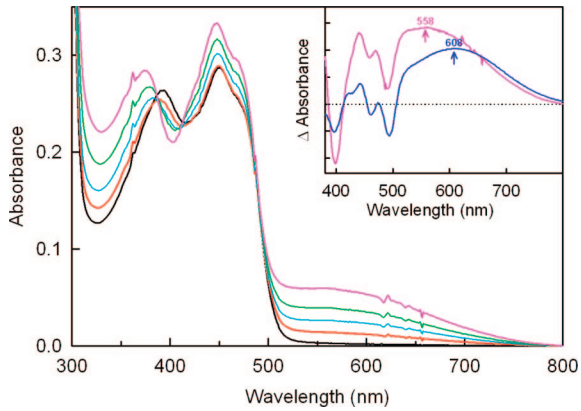

FIGURE 3: Spectral titration of the Arg49Lys mutant with pyrrole-2-carboxylate (PCA). The black curve is the absorption spectrum of the Arg49Lys mutant (20.4 μM) in 50 mM potassium phosphate buffer, pH 8.0, at 27 °C. The red, cyan, and green curves were recorded after addition of 9.9, 35.2, and 104 mM PCA, respectively. The magenta curve is the spectrum calculated for 100% complex formation as described in Experimental Procedures. The inset compares difference spectra calculated for 100% complex formation with Arg49Lys (magenta curve) and the wild-type enzyme (blue curve). The data for wild-type enzyme were taken from Wagner et al. (*1*) and are normalized to the same concentration as the mutant.

band in the visible absorption spectrum (*29*). The pK_a for N(3)H ionization in FAD bound to wild-type MSOX (pK_a = 8.3) is more than 2 pH units lower than that observed with free flavin (pK_a = 10.4) (*1*). Ionization of FAD bound to the Arg49Lys mutant is also detectable, as judged by the 10 nm hypsochromic shift of the 393 nm absorption band when the pH is raised from 8.0 to more alkaline values (Figure 4A). The pK_a for N(3)H ionization in the mutant enzyme is, however, dramatically increased as compared with wild-type MSOX (Figure 4B). In fact, the mutant exhibits a pK_a value identical to that observed with free flavin (Table 3).

Photoreduction of the Arg49Lys Mutant. Photoreduction of wild-type MSOX results in the quantitative formation of a red anionic flavin radical, followed by a slower reaction that generates fully reduced flavin (*1*). Photoreduction of the Arg49Lys mutant results in the isosbestic conversion of oxidized enzyme to a species that exhibits an intense absorption band at 387 nm (ϵ_{387} = 25600 M^{-1} cm^{-1}) plus a second weaker band at 475 nm (Figure 5). The spectral properties of the intermediate are characteristic of those observed for anionic flavin radicals (*30*). Further irradiation leads to an isosbestic conversion of the mutant radical to fully reduced flavin (Figure 5, inset). The results indicate that photoreduction of the Arg49Lys mutant

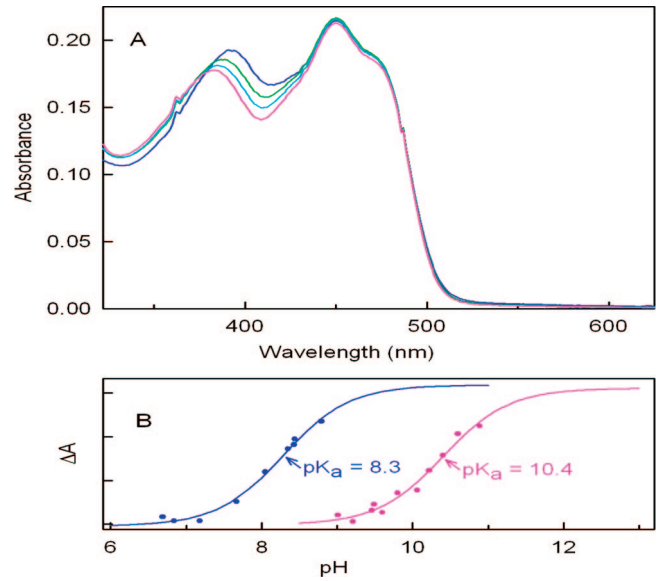

FIGURE 4: Effect of pH on the absorption spectrum of the Arg49Lys mutant. Panel A: Spectra were recorded at 10 °C in 100 mM potassium pyrophosphate (pH ≤9.49) or 100 mM sodium carbonate (pH ≥9.49). The blue, green, cyan, and magenta curves show spectra recorded at pH 8.76, 10.06, 10.40, and 10.89, respectively. Panel B: Absorbance changes observed with the Arg49Lys mutant at 400 nm (magenta circles) or wild-type MSOX at 352 nm (blue circles) are plotted as a function of pH. The magenta and blue lines were obtained by fitting an equation for a pH titration curve [$\Delta A = (A[H^+] + BK_a)/([H^+] + K_a)$, where A and B are the calculated ΔA at low and high pH, respectively] to data obtained with mutant and wild-type MSOX, respectively. The data for the wild-type enzyme were previously reported (*1*).

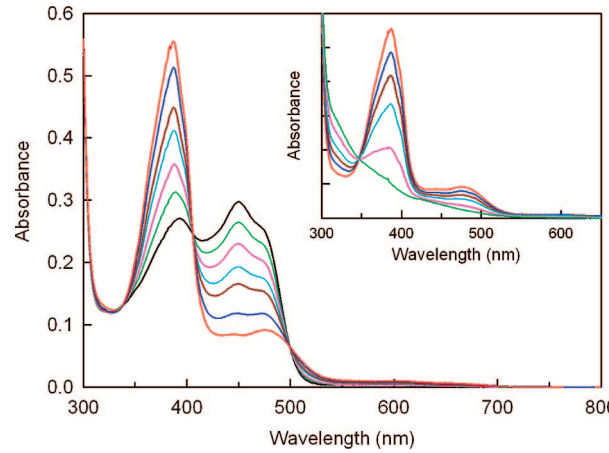

FIGURE 5: Photoreduction of the Arg49Lys mutant. The black curve is the absorption spectrum of the oxidized enzyme in anaerobic 10 mM potassium phosphate buffer, pH 8.0, containing 8 mM EDTA, 0.25 μM 5-deazariboflavin, and 25 μM methyl viologen. Green, magenta, cyan, brown, blue, and red curves were recorded after illumination for 16, 31, 39, 45, 60, and 77 min, respectively. The inset shows the conversion of the radical to the fully reduced enzyme. Red, blue, brown, cyan, magenta, and green curves were recorded after 77, 120, 157, 221, 346, and 496 min, respectively.

proceeds via an anionic radical intermediate, similar to that observed with wild-type MSOX (*1*).

Reduction Potentials. The 1-electron reduction potential for the OX/RAD couple with wild-type MSOX is about 400 mV more positive than that observed with free flavin, as judged by results obtained in a previous study (E_1 = 79.5 ± 0.2 mV, pH 8.0) (*31*) using the xanthine oxidase spectro-

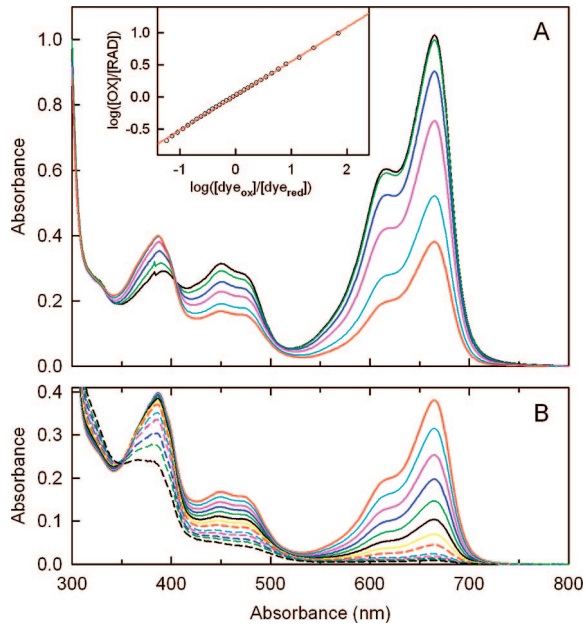

FIGURE 6: Determination of the 1-electron reduction potential for the OX/RAD couple (E_1) with the Arg49Lys mutant at pH 8.0. The reaction was conducted using 20 μM methylene blue as the indicator dye. [At this concentration the dye exhibits minimal absorbance (<0.04) in the 350−500 nm region.] For clarity, spectra recorded during the initial ($t \leq 73$ min) and latter ($t \geq 73$ min) parts of the reaction are shown in panels A and B, respectively. Panel A: Black, green, blue, magenta, cyan, and red curves were recorded 0, 5, 17, 33, 57, and 73 min, respectively, after addition of xanthine oxidase. The inset in panel A shows a plot of log([OX]/[RAD]) versus log([dye$_{ox}$]/[dye$_{red}$]). Panel B: Spectra shown as red, cyan, magenta, blue, green, black, and yellow solid lines were recorded 73, 81, 89, 97, 105, 113, and 121 min, respectively, after xanthine oxidase addition. Spectra shown as red, cyan, magenta, blue, green, and black dashed lines were recorded 129, 143, 153, 173, 193, and 233 min, respectively, after xanthine oxidase addition.

photometric method described by Massey (*20*) with toluylene blue as the redox indicator dye (E_m = 81.3 mV, pH 8.0). The high potential for the OX/RAD couple was confirmed when the measurement with wild-type MSOX was repeated in the present study (E_1 = 82.2 ± 0.3 mV).

Attempts to measure E_1 with the Arg49Lys mutant under the same conditions suggested that the potential of the mutant enzyme was considerably lower than wild-type MSOX because the xanthine oxidase-mediated reduction of toluylene blue was complete before significant reduction of the mutant was detected. A value for E_1 with the Arg49Lys mutant could be determined by using an indicator dye, methylene blue, with a lower potential (E_m = −20.0 mV, pH 8.0) (Figure 6). The value obtained with the mutant (E_1 = −21.0 ± 0.1 mV) is 100 mV more negative than that observed with wild-type MSOX (Table 3).

Partial conversion of the mutant radical to fully reduced flavin occurred prior to complete reduction of the indicator dye in the reaction observed with methylene blue. The data were used to obtain a preliminary estimate of the potential for the RAD/RED couple ($E_2 \sim -50$ mV). The reaction with the mutant enzyme was repeated using pyocyanine as the indicator dye (E_m = −87.6 mV, pH 8.0) (Figure 7). The potential calculated for the RAD/RED couple based on the pyocyanine data (E_2 = −47.4 ± 0.2 mV) is consistent with the methylene blue estimate. The separation between the two

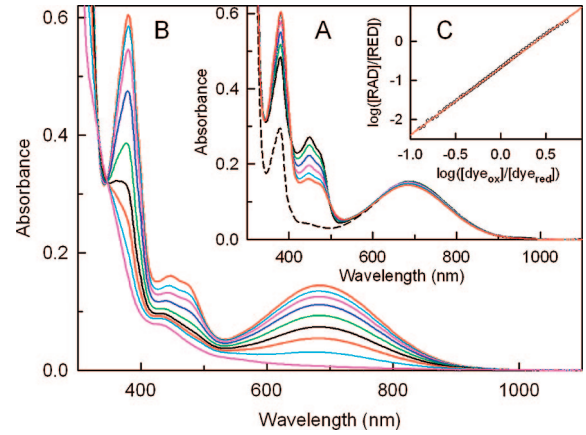

FIGURE 7: Determination of the 1-electron reduction potential for the RAD/RED couple (E_2) with the Arg49Lys mutant at pH 8.0. The reaction was conducted using 60 μM pyocyanine as the indicator dye. For clarity, spectra recorded during the initial ($t \leq 30$ min) and latter ($t \geq 30$ min) part of the reaction are shown in panels A and B, respectively. Panel A: The absorption spectrum of pyocyanine (dotted black line) was recorded before adding Arg49Lys MSOX or xanthine oxidase. The solid black curve was recorded after addition of the MSOX mutant. The green, blue, magenta, cyan, and red curves were recorded 6, 12, 18, 24, and 30 min, respectively, after addition of xanthine oxidase. Panel B: The red, cyan, magenta, blue, green, black, and the bottom-most red, cyan, and magenta curves were recorded 30, 42, 54, 72, 96, 120, 144, 176, and 302 min, respectively, after addition of xanthine oxidase. Panel C shows a plot of log([RAD]/[RED]) versus log([dye$_{ox}$]/[dye$_{red}$]).

reduction potentials ($E_1 - E_2 = \Delta E$) was used to calculate the radical formation constant [ΔE (mV) = 59 log K, K = [RAD]^2/[OX][RED]]. The radical yield expected upon 50% reduction of the Arg49Lys mutant can be estimated using the value obtained for the radical formation constant (K = 2.8). The predicted value (46%) is in good agreement with the value observed in the methylene blue reaction (49%). The results suggest that the quantitative radical formation observed during photoreduction of the mutant is attributable to kinetic stabilization.

Unlike the mutant, a reliable value for the potential of the RAD/RED couple with the wild-type enzyme was not obtained despite extensive studies with various indicator dyes and different levels of xanthine oxidase. The reason for this outcome is unclear but may reflect very slow equilibration of reducing equivalents between the enzyme and indicator dye.

Crystal Structure Analysis of the Arg49Lys Mutant. The Arg49Lys mutant was crystallized under precipitating conditions of high salt ("phosphate" crystals) or high PEG ("PEG" crystals) concentration. The cell parameters of the "phosphate" crystals were similar to other native, ligand-bound and mutant MSOX crystals prepared earlier, while those of the "PEG" crystals exhibited a 6 Å longer c axis and 2° larger monoclinic β angle. Both diffracted well (1.7 and 2.1 Å, respectively), a range similar to other MSOX structures. Both crystals contained two chloride ions, bound in the center of the molecule near the ribityl phosphate of each FAD. In addition, the "phosphate" crystal contained two molecules of glycerol (the cryoprotectant), one bound to each molecule in the asymmetric unit; the "PEG" crystal contained none. The "PEG" crystal contained three residues in alternate conformations (Arg154 of each molecule and Ser112 of the

Table 4: Comparison of Arg49Lys Crystals with Wild-Type MSOX

crystal	molecule	active site loop (56−60)	external loop (186−191)
"phosphate" Arg49Lys	1	closed	A configuration
	2	closed	B configuration
"PEG" Arg49Lys	1	open	A configuration
	2	closed	A configuration
wild type[a]	1	open	A configuration
	2	closed	B configuration

[a] Ligand-free wild-type MSOX (PDB entry 2GBO).

second molecule) while the "phosphate" crystal had none. Both crystals contained two residues in disallowed conformations (Asp47 of each molecule), a feature common to all structures of MSOX from *Bacillus* sp. B-0618 determined to date (*1, 14, 31*).

When the two independent molecules of the "phosphate" Arg49Lys mutant are aligned, the RMSD for equivalent Cα atoms is 0.29 Å when the first two residues are omitted. Comparison of the two molecules of the "PEG" mutant after alignment shows an RMSD of 0.39 Å, again with the first two residues omitted.

The only significant difference in backbone structure between the two molecules in the "phosphate" mutant crystal is in the segment 186–191 (up to 2.7 Å deviation), an external loop that is sensitive to the crystal packing environment and is consistently different between the two molecules in crystals of MSOX from *Bacillus* sp. B-0618 examined in previous studies: molecule 1, A configuration; molecule 2, B configuration (Table 4). In contrast, the external 186–191 loop is in the A configuration and very similar in the two molecules in the "PEG" mutant crystal (differing by ~0.6 Å), consistent with an altered crystal packing arrangement of the "PEG" crystal compared to the "phosphate" crystal.

The only significant backbone conformational difference between the two molecules in the "PEG" mutant crystal is in the peptide segment 56–60 (up to 2.99 Å deviation), a loop that controls access to the solvent-filled active site cavity. The active site loop is open in molecule 1 and closed in molecule 2 in the "PEG" mutant crystal whereas the loop is found only in the closed conformation in both molecules in the "phosphate" mutant crystal (Table 4).

Structural Comparison with Wild-Type MSOX. Our previous studies with ligand-free wild-type MSOX (PDB entry 2GB0) show that the active site loop is flexible. In the wild-type structure, the active site loop is open in molecule 1 and closed in molecule 2 (*11*), as observed for the "PEG" mutant crystal. When molecules 1 and 2 in the "phosphate" mutant crystal are compared to molecules 1 and 2, respectively, in ligand-free wild-type MSOX, the RMSD for molecule 1 is 0.35 Å with a substantial difference in the active site loop while for molecule 2 the RMSD is 0.16 Å with no substantial difference between them. A similar comparison of the "PEG" mutant crystal with wild-type MSOX shows an RMSD of 0.21 Å and no substantial differences of any segments in molecule 1 and an RMSD of 0.33 Å with substantial differences only in the surface 186–191 loop in molecule 2.

The conformations of the side chains in the immediate vicinity of the flavin ring are also highly conserved among the wild-type enzyme and the "phosphate" and "PEG" Arg49Lys mutants. The side chain of Lys49 is nearly congruent to that of the wild-type Arg49, with the terminal

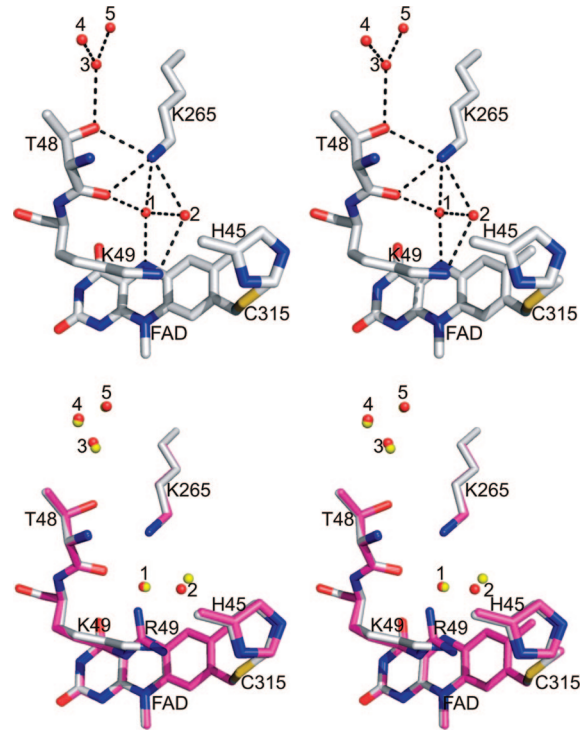

FIGURE 8: The top panel shows a stereoview of the region above the *si* face of the flavin ring in the "phosphate" crystal of the Arg49Lys mutant (molecule 1, active site loop closed). Carbon atoms are shown in white, oxygens are in red, nitrogens are in blue, and the sulfur is in yellow. Waters are shown as red balls. (Wat4 is in contact with bulk solvent.) Hydrogen bonds are indicated by dotted lines. The bottom panel is a stereoview of the same region of the mutant superimposed with that observed for wild-type MSOX (PDB entry 2GBO, molecule 2, active site loop closed). Atoms are colored as indicated in the top panels except carbons and waters in wild-type MSOX are colored magenta and yellow, respectively.

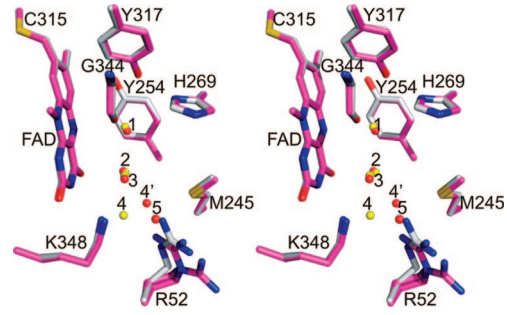

FIGURE 9: Stereoview comparison of the region above the *re* face of the flavin ring in the "phosphate" crystal of the Arg49Lys mutant (molecule 2, active site loop closed) and wild-type MSOX (PDB entry 2GBO, molecule 2, active site loop closed). Carbon atoms are colored white and magenta in the mutant and wild-type structures, respectively. In both structures, oxygens are in red, nitrogens are in blue, and sulfur is in yellow. Waters are shown as yellow or red balls in the mutant and wild-type structures, respectively. The side chain of Arg52 in wild-type MSOX is modeled in two alternate configurations; wat5 is present at half-occupancy.

NZ atom forming very similar interactions with the isoalloxazine ring, nearby side chains, and water molecules that are located on the *si* face of the flavin ring (Figure 8). The active site cavity in MSOX is located on the *re* face of the flavin ring. The only significant differences in this region are in the orientation of the Arg52 side chain, which binds

to the carboxylate group of substrate analogues (*1, 14*), and in the active site water structure. In the closed form of ligand-free wild-type MSOX (molecule 2, Table 4), the side chain of Arg52 is found to be in two alternate conformations, one pointing toward the flavin ring ("in") and the other pointing away ("out") (Figure 9). The active site cavity in wild-type MSOX contains five water molecules. One of the water molecules (wat5) is present at half-occupancy, its position being occluded by the "in" conformation of the Arg52 side chain. In both molecules of the "phosphate" mutant crystal the Arg52 side chain occupies only a single conformation. This conformation is similar to, but slightly different from, that of the "in" conformation of Arg52 in the closed form of the ligand-free wild-type enzyme. The active site cavity in the "phosphate" mutant crystal contains only four water molecules, the fifth putative water site being occluded by the "in" conformation of the Arg52 side chain (Figure 9). One of the other four water molecules in the mutant active site cavity is displaced from its wild-type position because of the slight difference in position of the Arg52 side chain. In the closed form of the "PEG" mutant crystal the Arg52 side chain is oriented similarly to that in the "phosphate" mutant crystal, but only two of the active site waters are visible.

DISCUSSION

Catalytic and Structural Properties of the Arg49Lys Mutant. Mutation of Arg49 to Lys results in a 40-fold decrease in k_{cat} and a 150-fold decrease in $k_{cat}/K_{m\ sarcosine}$. Previous studies with wild-type MSOX show that the limiting rate of anaerobic reduction with sarcosine is just slightly larger than k_{cat}, suggesting that the reductive half-reaction is at least partly rate-limiting during turnover (*11*). The overall structure of the Arg49Lys mutant is very similar to that observed for ligand-free wild-type MSOX. The side chain of Lys49 is in van der Waals contact with the *si* face of the flavin ring and is nearly congruent to that of Arg49 in wild-type MSOX.

The only significant backbone structural differences between the mutant and wild-type enzymes are in the active site loop (residues 55–60) and the external loop (residues 186–191) (Table 4). The external loop variations between molecules 1 and 2 among the wild-type and mutant crystals can be fully explained as crystal packing artifacts. The "phosphate" mutant structure and all other MSOX structures previously studied in this laboratory are isomorphous, and the observed difference in external loop configuration in molecules 1 (A configuration) and 2 (B configuration) can be attributed to differences in crystal packing. Only in the "PEG" crystal, which is nonisomorphous to all the others and in which the crystal packing near the loop is different, do both molecules adopt the A configuration. Therefore, the difference in the catalytic properties cannot be caused by this structural difference.

In all ligand-bound forms of MSOX previously studied in this laboratory, the active site loop on the *re* face of the flavin ring (residues 55–60) in both molecules in the asymmetric unit is in the closed configuration. This configuration is stabilized by cooperative hydrogen bonding and charge–charge interactions involving side chains that interact with the ligand molecule (*1, 14, 31*). However, in the ligand-free wild-type enzyme this loop is found to be open in molecule 1 and closed in molecule 2 (Table 4). Therefore, in the absence of a ligand to stabilize the closed configuration, this loop is able to take up either the closed or open configuration in the wild-type enzyme. In the "phosphate" Arg49Lys mutant the 55–60 loop of both molecules is in the closed configuration while in the "PEG" mutant crystal the loop configuration is similar to that of the wild-type enzyme with molecule 1 open and molecule 2 closed. Overall, the results suggest that, in the absence of ligand, the configuration of the 55–60 loop in the wild-type or mutant enzyme is essentially arbitrary, with little difference in stabilization energy. We conclude that structural differences observed at the active site loop are very unlikely to explain the observed differences in catalytic activity. It is also unlikely that the slight differences in the water structures or in the orientation of the Arg52 side chains of the closed forms of the Arg49Lys mutant enzyme is responsible for its reduced catalytic activity.

Biophysical Properties of the Active Site in the Arg49Lys Mutant. The pK_a for N(3)H ionization in oxidized FAD bound to the Arg49Lys mutant is shifted up by more than 2 pH units as compared with wild-type MSOX. The higher pK_a value is consistent with a less electropositive active site in the mutant that reduces the stability of the oxidized flavin anion as compared with wild-type MSOX. The charge transfer bands observed for the MTA or PCA complexes with the Arg49Lys mutant absorb at higher energy than those observed for the corresponding wild-type complexes. Oxidized FAD and the ligand act as partial electron acceptor and donor, respectively, in all of the observed charge transfer complexes. The absorption energy of a charge transfer band in complexes formed between the same donor and different acceptors (i.e., FAD in mutant and wild-type MSOX) should be inversely proportional to the 1-electron reduction potential of the acceptor. The observed differences in charge transfer band energies suggested that the Arg49Lys mutation caused a decrease in the reduction potential of the OX/RAD couple. Indeed, we found that the potential of the OX/RAD couple in the mutant is 100 mV lower than in the wild-type enzyme. This outcome is also consistent with a less electropositive active site in the mutant enzyme. The observed decrease in the reduction potential of the mutant enzyme is likely to be a major cause of its reduced catalytic activity.

A Context-Sensitive Model for the Electrostatic Impact of Arginine to Lysine Mutations. Although lysine is generally regarded as a conservative substitute for arginine, the two amino acid side chains exhibit a significant difference in basicity. In the absence of a nearby negative charge, desolvation effects are likely to decrease the pK_a of an arginine or a lysine residue in a protein, as compared to that observed for free arginine or lysine in aqueous solution (pK_a = 12.5 and 10.5, respectively) (*32*). A several pH unit decrease in pK_a owing to desolvation, coupled with the inherent difference in the basicity of arginine and lysine, could result in a major disparity in the protonation state at physiological pH of lysine in the mutant as compared with the corresponding arginine in the wild-type enzyme. Consequently, a more electropositive environment is expected in the vicinity of the protonated arginine in the wild-type enzyme as compared with that near the unprotonated lysine in the mutant at physiological pH.

The presence of a nearby negative charge will, however, dramatically alter the electrostatic impact of an arginine to lysine mutation. In this case, charge–charge interactions are likely to be the main determinant of pK_a value and are expected to increase the pK_a of an arginine or a lysine residue. This will negate inherent differences in the basicity of the side chains of the two amino acids with respect to their protonation state at physiological pH. Consequently, the model would predict a similar electrostatic environment near the protonated arginine or lysine in the wild-type or mutant enzyme, respectively.

The context-sensitive model can account for the opposite effects of the Arg49 to Lys mutation in (1) the MSOX holoenzyme that contains covalently bound FAD and (2) the noncovalent enzyme·FAD complex that is formed as an intermediate during holoenzyme biosynthesis. Case 1: Desolvation effects predominate in the holoenzyme; the side chain of residue 49 is protonated at physiological pH in the wild-type enzyme but unprotonated in the Arg49Lys mutant. Electrostatic interaction between the positively charged side chain of Arg49 and the oxidized flavin increases the potential of the OX/RAD couple and lowers the pK_a for ionization at flavin N(3) in wild-type MSOX as compared with the mutant where electrostatic stabilization is minimal because the side chain of Lys49 is unprotonated. Case 2: Charge–charge interactions predominate in the noncovalent flavinylation intermediate where the side chain of residue 49 is close to Cys315, the site of covalent flavin attachment in the holoenzyme. These interactions raise the pK_a of Arg49 or Lys49 and lower the pK_a for ionization of Cys315, generating the thiolate form of the wild-type or mutant intermediate that is required for covalent attachment to the 8α-methyl group of FAD (*15*). Consequently, the mutation is not expected to affect the kinetics of covalent flavinylation, as observed.

What Is the Catalytic Function of Arg49? There is no direct contact between Arg49 and sarcosine because they are separated by the flavin ring. The Arg49 side chain is in van der Waals contact with the *si* face while the substrate binds in van der Waals contact to the *re* face. Nevertheless, Arg49 plays an important role in sarcosine oxidation by virtue of its electrostatic effect on the active site environment. First, the positively charged guanidinium side chain in contact with the flavin ring raises the flavin reduction potential and thereby facilitates sarcosine oxidation. An additional role for Arg49 in sarcosine oxidation is suggested by the fact that MSOX is known to bind the unreactive zwitterionic form of its amino acid substrates. Substrate activation is achieved by inducing a large decrease in the pK_a of the bound zwitterion (*10, 11*). Electrostatic interaction of the reactive substrate anion with the positively charged side chain of Arg49 may contribute to the observed shift in the pK_a of the bound amino acid.

Concluding Remarks. Although sarcosine oxidation by the MSOX holoenzyme is more than 4 orders of magnitude faster than covalent flavinylation of the apoenzyme, the reactions exhibit a surprising number of common features. Both sarcosine oxidation and covalent flavinylation produce a covalently bound reduced flavin intermediate. In each case, the intermediate is rapidly oxidized by molecular oxygen with the concomitant production of a stoichiometric amount of hydrogen peroxide. Electrostatic interactions with Arg49 play an important role in both catalysis and covalent flavinylation. Covalent flavin attachment at Cys315 is blocked by the absence of a basic residue at position 49 but is scarcely affected by mutation of Arg49 to Lys (*15*). In contrast, the same mutation results in a large decrease in catalytic activity. The dramatically different consequences of the Arg49Lys mutation on catalysis and covalent flavinylation are attributed to the absence and presence, respectively, of the negatively charged thiolate side chain of Cys315, as described in a model where the electrostatic impact of an arginine to lysine mutation varies depending on the local environment. The identification of Arg49 as a bifunctional residue important in the biosynthesis and catalytic properties of the MSOX holoenzyme provides insight as to how a single active site may have evolved that efficiently catalyzes both an autoflavinylation reaction and the oxidation of secondary amino acids.

ACKNOWLEDGMENT

We thank Russ Hille for the generous gift of xanthine oxidase.

REFERENCES

1. Wagner, M. A., Trickey, P., Chen, Z., Mathews, F. S., and Jorns, M. S. (2000) Monomeric sarcosine oxidase: 1. Flavin reactivity and active site binding determinants. *Biochemistry 39*, 8813–8824.
2. Wagner, M. A., and Jorns, M. S. (2000) Monomeric sarcosine oxidase: 2. Kinetic studies with sarcosine, alternate substrates and substrate analogs. *Biochemistry 39*, 8825–8829.
3. Wagner, M. A., Khanna, P., and Jorns, M. S. (1999) Structure of the flavocoenzyme of two homologous amine oxidases: Monomeric sarcosine oxidase and *N*-methyltryptophan oxidase. *Biochemistry 38*, 5588–5595.
4. Khanna, P., and Jorns, M. S. (2001) Characterization of the FAD-containing *N*-methyltryptophan oxidase from *Escherichia coli*. *Biochemistry 40*, 1441–1450.
5. Venci, D., Zhao, G., and Jorns, M. S. (2002) Molecular characterization of nikD, a new flavoenzyme important in the biosynthesis of nikkomycin antibiotics. *Biochemistry 41*, 15795–15802.
6. Dodt, G., Kim, D. G., Reimann, S. A., Reuber, B. E., McCabe, K., Gould, S. J., and Mihalik, S. J. (2000) L-pipecolic acid oxidase, a human enzyme essential for the degradation of L-pipecolic acid, is most similar to the monomeric sarcosine oxidases. *Biochem. J. 345*, 487–494.
7. Wu, X. L., Takahashi, M., Chen, S. G., and Monnier, V. M. (2000) Cloning of amadoriase I isoenzyme from *Aspergillus* sp.: Evidence of FAD covalently linked to Cys342. *Biochemistry 39*, 1515–1521.
8. Hassan-Abdallah, A., Bruckner, R. C., Zhao, G., and Jorns, M. S. (2005) Biosynthesis of covalently bound flavin: Isolation and in vitro flavinylation of the monomeric sarcosine oxidase apoprotein. *Biochemistry 44*, 6452–6462.
9. Zhao, G., and Jorns, M. S. (2002) Monomeric sarcosine oxidase: Evidence for an ionizable group in the ES complex. *Biochemistry 41*, 9747–9750.
10. Zhao, G., and Jorns, M. S. (2005) Ionization of zwitterionic amine substrates bound to monomeric sarcosine oxidase. *Biochemistry 44*, 16866–16874.
11. Zhao, G., and Jorns, M. S. (2006) Spectral and kinetic characterization of the Michaelis charge transfer complex in monomeric sarcosine oxidase. *Biochemistry 45*, 5985–5992.
12. Zhao, G., Qu, J., Davis, F. A., and Jorns, M. S. (2000) Inactivation of monomeric sarcosine oxidase by reaction with *N*-(cyclopropyl)glycine. *Biochemistry 39*, 14341–14347.
13. Chen, Z., Zhao, G., Martinovic, S., Jorns, M. S., and Mathews, F. S. (2005) Structure of the sodium borohydride-reduced *N*-(cyclopropyl)glycine adduct of the flavoenzyme monomeric sarcosine oxidase. *Biochemistry 44*, 15444–15450.
14. Trickey, P., Wagner, M. A., Jorns, M. S., and Mathews, F. S. (1999) Monomeric sarcosine oxidase: Structure of a covalently-flavinylated secondary amine oxidizing enzyme. *Structure 7*, 331–345.

15. Hassan-Abdallah, A., Zhao, G., and Jorns, M. S. (2007) Covalent flavinylation of monomeric sarcosine oxidase: Identification of a residue essential for holoenzyme biosynthesis. *Biochemistry* (in press).
16. O'Brien, D. E., Weinstock, L. T., and Cheng, C. C. (1970) Synthesis of 10-deazariboflavin and related 2,4-dioxopyrimido[4,5-*b*]quinolines. *J. Heterocycl. Chem. 7*, 99–105.
17. McIlwain, H. (1937) The phenazine series. Part VI. Reactions of alkyl phenazonium salts; the phenazyls. *J. Chem. Soc. 2*, 1704–1711.
18. Pace, C. P., and Stankovich, M. T. (1987) Redox properties of electron-transferring flavoprotein from *Megasphaera elsdenii*. *Biochim. Biophys. Acta 911*, 267–276.
19. Hassan-Abdallah, A., Zhao, G., and Jorns, M. S. (2006) Role of the covalent flavin linkage in monomeric sarcosine oxidase. *Biochemistry 45*, 9454–9462.
20. Massey, V. (1991) A simple method for the determination of redox potentials, in *Flavins and Flavoproteins* (Curti, B., Ronchi, S., and Zanetti, G., Eds.) pp 59–66, de Gruyter, Berlin.
21. Clark, W. M. (1960) *Oxidation-reduction potential of organic systems*, Williams and Wilkins, Baltimore, MD.
22. Prince, R. C., Linkletter, S. J. G., and Dutton, P. L. (1981) The thermodynamic properties of some commonly used oxidation-reduction mediators, inhibitors and dyes as determined by polarography. *Biochim. Biophys. Acta 635*, 132–148.
23. Otwinowski, Z., and Minor, W. (1997) Processing of X-ray diffraction data collected in oscillation mode. *Methods Enzymol. 276*, 307–326.
24. Collaborative Computational Project, Number 4 (1994) The CCP4 suite: Programs for protein crystallography,*Acta Crystallogr. D50*, 760–763.
25. Brünger, A. T., Adams, P. D., Clore, G. M., DeLano, W. L., Gros, P., Grosse-Kunstleve, R. W., Jiang, J. S., Kuszewski, J., Nilges, M., Pannu, N. S., Read, R. J., Rice, L. M., Simonson, T., and Warren, G. L. (1998) Crystallography & NMR system: A new software suite for macromolecular structure determination. *Acta Crystallogr. D54*, 905–921.
26. Kleywegt, G. J., and Brünger, A. T. (1996) Checking your imagination: Application of the free r value. *Structure 4*, 897–904.
27. Jiang, J.-S., and Brünger, A. T. (1994) Protein hydration observed by X-ray diffraction solvation properties of penicillopepsin and neuraminidase crystal structures. *J. Mol. Biol. 243*, 100–115.
28. Roussel, A., and Cambillau, C. (1991) TURBO-FRODO, in *Silicon Graphics Geometry Partners Directory 86*, Silicon Graphics, Mountain View, CA.
29. Massey, V., and Ganther, H. (1965) On the interpretation of the absorption spectra of flavoproteins with special reference to D-amino acid oxidase. *Biochemistry 4*, 1161–1173.
30. Massey, V., and Palmer, G. (1966) On the existence of spectrally distinct classes of flavoprotein semiquinones. A new method for the quantitative production of flavoprotein semiquinones. *Biochemistry 5*, 3181–3189.
31. Zhao, G., Song, H., Chen, Z., Mathews, F. S., and Jorns, M. S. (2002) Monomeric sarcosine oxidase: Role of histidine 269 in catalysis. *Biochemistry 41*, 9751–9764.
32. Li, H., Robertson, A. D., and Jensen, J. H. (2005) Very fast empirical prediction and rationalization of protein pK_a values. *Proteins 61*, 704–721.

BI702351V